

A correlation between the stellar and [Fe II] velocity dispersions in Active Galaxies

Rogemar. A. Riffel^{1*}, Thaisa Storchi-Bergmann², Rogério Riffel², Miriani G. Pastoriza², Alberto Rodríguez-Ardila³, Oli L. Dors Jr⁴, Jaciara Fuchs¹, Marlon R. Diniz¹, Schönell, A. J. Júnior¹, Moiré G. Hennig¹, Carine Brum¹

¹ *Universidade Federal de Santa Maria, Departamento de Física/CCNE, 97105-900, Santa Maria, RS, Brazil*

² *Universidade Federal do Rio Grande do Sul, Instituto de Física, CP 15051, Porto Alegre 91501-970, RS, Brazil.*

³ *Laboratório Nacional de Astrofísica/MCT, Rua dos Estados Unidos 154, Itajubá, MG, Brazil.*

⁴ *Universidade do Vale do Paraíba, Av. Shishima Hifumi 2911,12244-000, São José dos Campos SP, Brazil.*

2 January 2018

ABSTRACT

We use near-infrared spectroscopic data from the inner few hundred parsecs of a sample of 47 active galaxies to investigate possible correlations between the stellar velocity dispersion (σ_*), obtained from the fit of the K-band CO stellar absorption bands, and the gas velocity dispersion (σ) obtained from the fit of the emission-line profiles of [S III] λ 0.953 μ m, [Fe II] λ 1.257 μ m, [Fe II] λ 1.644 μ m and H₂ λ 2.122 μ m. While no correlations with σ_* were found for H₂ and [S III], a good correlation was found for the two [Fe II] emission lines, expressed by the linear fit $\sigma_* = 95.4 \pm 16.1 + (0.25 \pm 0.08) \times \sigma_{[\text{Fe II}]}$. Excluding barred objects from the sample a better correlation is found between σ_* and $\sigma_{[\text{Fe II}]}$, with a correlation coefficient of $R = 0.80$ and fitted by the following relation: $\sigma_* = 57.9 \pm 23.5 + (0.42 \pm 0.10) \times \sigma_{[\text{Fe II}]}$. This correlation can be used to estimate σ_* in cases it cannot be directly measured and the [Fe II] emission lines are present in the spectra, allowing to obtain the mass of the supermassive black hole (SMBH) from the $M_\bullet - \sigma_*$ relation. The scatter from a one-to-one relationship between σ_* and its value derived from $\sigma_{[\text{Fe II}]}$ using the equation above for our sample is 0.07 dex, which is smaller than that obtained in previous studies which use $\sigma_{[\text{O III}]}$ in the optical as a proxy for σ_* . The use of $\sigma_{[\text{Fe II}]}$ in the near-IR instead of $\sigma_{[\text{O III}]}$ in the optical is a valuable option for cases in which optical spectra are not available or are obscured, as is the case of many AGN.

The comparison between the SMBH masses obtained using the $M_{\bullet} - \sigma_{\star}$ relation in which σ_{\star} was directly measured with those derived from $\sigma_{[\text{Fe II}]}$ reveals only a small average difference of $\Delta \log M_{\bullet} = 0.02$ with a scatter of 0.32 dex for the complete sample and $\Delta \log M_{\bullet} = 0.00$ with a scatter of 0.28 dex for a sub-sample excluding barred galaxies.

Key words: galaxies: active – galaxies: nuclei – infrared: galaxies – black holes

1 INTRODUCTION

In the present paradigm of galaxy evolution, most galaxies which form a bulge also form a supermassive black hole (SMBH) in their nuclei (e.g. Magorrian et al. 1998; Richstone et al. 1998; Ferrarese & Merrit 2000; Gebhardt et al. 2000). The central SMBH seems to play a fundamental role in the galaxy evolution and cosmological simulations without considering the presence of a SMBH and its associated feedback predict masses for the galaxies much higher than those observed (Di Matteo, Springel & Hernquist 2005; Springel, Di Matteo & Hernquist 2005; Bower et al. 2006). In a scenario of co-evolution of the SMBH and its host galaxy, mass accretion to the central region of the galaxy leads to the growth of the galaxy bulge, while the feeding of the SMBH triggers episodes of nuclear activity which results in feedback in the form of radiation pressure and mass ejections from the accretion disk surrounding the SMBH. This episodic feedback may halt the mass accretion to the galaxy preventing its growth in the active phase (Nemmen et al. 2007). This co-evolution may be the mechanism which leads to the empirical relation between the mass of the SMBH and the stellar velocity dispersion of the bulge $M_{\bullet} - \sigma_{\star}$, [Ferrarese & Ford (2005); but see also Jahnke & Maccio (2011)].

The $M_{\bullet} - \sigma_{\star}$ relation has been extensively used to estimate the mass of SMBHs from the stellar kinematics, as direct determinations for the SMBH masses only are possible for the closest galaxies for which the radius of influence of the SMBH can be resolved (e.g. Ferrarese & Ford 2005). Although allowing to estimate the masses of the SMBHs for a large number of galaxies, the use of the $M_{\bullet} - \sigma_{\star}$ relation requires the measurement of σ_{\star} , which is not always easy to obtain, particularly in active galaxies, where the AGN continuum dilutes the stellar absorption lines. In order to overcome this difficulty, a number of scaling relations using the width and luminosities of emission lines to determine M_{\bullet} have been proposed (e.g. Booth & Schaye 2011; Wu 2009; Peterson 2008; Salviander et al. 2006; Vestergaard & Peterson 2006; Greene & Ho 2006, 2005; Kaspi et al.

2005; Onken et al. 2004; Nelson & Whittle 1996). Nevertheless, most of these relations are for the optical domain of the electromagnetic spectrum. With the improvement of infrared (IR) detectors, IR spectra of many AGNs have become recently available, and have the advantage of being less affected by reddening than optical spectra. In the present paper, we investigate the possibility of using the widths of emission lines in the near-IR as proxies for σ_* .

Recent studies by our group, using near-infrared (hereafter near-IR) integral field spectroscopy of active galaxies, have allowed the mapping of the flux distributions and kinematics of the molecular (H_2) and ionized gas. We have found, in particular, that the H_2 usually shows small velocity dispersions and a velocity field dominated by rotation, while the ionized gas shows higher velocity dispersions and is not dominated by rotation (e.g. Riffel et al. 2008, 2009; Riffel & Storchi-Bergmann 2011a,b). The kinematics and flux distributions are also consistent with a location for the H_2 gas in the galaxy plane, while the ionized gas, and, in particular [Fe II] extends to high galactic latitudes.

In the present paper we investigate the correlation between the gas and stellar kinematics derived from near-IR spectroscopy, with the goal of looking for a "proxy" for σ_* among the brightest emission lines in this wavelength range. This paper is organized as follows: in Section 2, we describe the sample and the observational data; in Section 3 we describe the methods used to measure the stellar and gaseous velocity dispersion. The results are presented in Section 4 and discussed in Section 5, while the conclusions are shown in Section 6.

2 OBSERVATIONAL DATA

The spectroscopic data used in this work are from Riffel, Rodríguez-Ardila & Pastoriza (2006); Rodríguez-Ardila, Contini & Viegas (2005) and Rodríguez-Ardila et al. (2004). The sample comprises 47 active galaxies with a range of activity types, and the spectra cover, on average, the inner 300 pc radius of the galaxies.

The near-infrared spectra were obtained with the NASA 3 m Infrared Telescope Facility (IRTF), using the SpeX spectrograph in the short cross-dispersed mode (SXD, 0.8-2.4 μm). The detector employed was a 1024 \times 1024 ALADDIN 3 InSb array with a spatial scale of 0.15"/pixel. A 0.8" \times 15" slit was used and the spectral resolution is 300 km s⁻¹, obtained from the measurement of the full width at half maximum (FWHM) of Arc lamp lines, or 127 km s⁻¹ in σ . The data reduction followed standard procedures. For more details on the instrumental configuration, data reduction, calibration processes and details of the extraction of the spectra see Riffel, Rodríguez-Ardila & Pastoriza (2006).

The above sample was chosen for this work because it is an unique dataset of near-IR spectroscopy of active galaxies, observed with the same instrumental setup (thus with no instrumental bias), covering the near-IR Z, J, H and K bands, and including several emission and absorption features allowing the comparison of the stellar and gas kinematics.

3 METHODS

In order to obtain the gaseous velocity dispersion σ , we fitted the emission-line profiles of [S III] λ 0.953 μ m, [Fe II] λ 1.257 μ m, [Fe II] λ 1.644 μ m and H₂ λ 2.122 μ m by single Gaussian curves and adopted as the measured velocity dispersion the σ of the Gaussian. These emission lines have been chosen because they are the strongest in the near-IR spectra of active galaxies (e.g. Riffel, Rodríguez-Ardila & Pastoriza 2006). We excluded the H and He recombination lines due to uncertainties in the fit for type 1 objects, for which is not always easy to separate the narrow from the broad components. The fitting of the emission-line profiles was done by adapting the PROFIT routine (Riffel 2010), which outputs the emission-line flux, the centroid velocity, the velocity dispersion and the uncertainties for each of these parameters. The velocity dispersion was then corrected for the instrumental $\sigma_{inst} = 127 \text{ km s}^{-1}$, which was subtracted in quadrature from the σ obtained from the fit of the Gaussians to the line profiles.

We measured the stellar velocity dispersion (σ_*) using the penalized Pixel-Fitting (pPXF) method of Cappellari & Emsellem (2004) in order to fit the CO absorptions bands at $\sim 2.3\mu$ m in the K-band. The pPXF method requires the use of stellar spectra as templates. We used for this the spectra of 60 late-type stars, 40 of them from the Gemini Near-IR Late-type stellar library (Winge, Riffel & Storchi-Bergmann 2009) and the remaining 20 spectra are from stars with public NIFS observations in the Gemini data archive (Diniz et al., 2012 in preparation). The uncertainties on the measurements of σ_* were estimated using 100 Monte-Carlo iterations as in Riffel & Storchi-Bergmann (2011b).

In order to illustrate our procedures, we show in Fig. 1 sample fits of the CO absorption band heads at 2.3μ m using the pPXF method, as well as fits of the emission-line profiles using PROFIT for the spectrum of the galaxy NGC5929.

4 RESULTS

The resulting measurements for the stellar and gas velocity dispersions for the galaxies of our sample are shown in Table 1. The dashes in the Table are due to the fact that for a few objects we

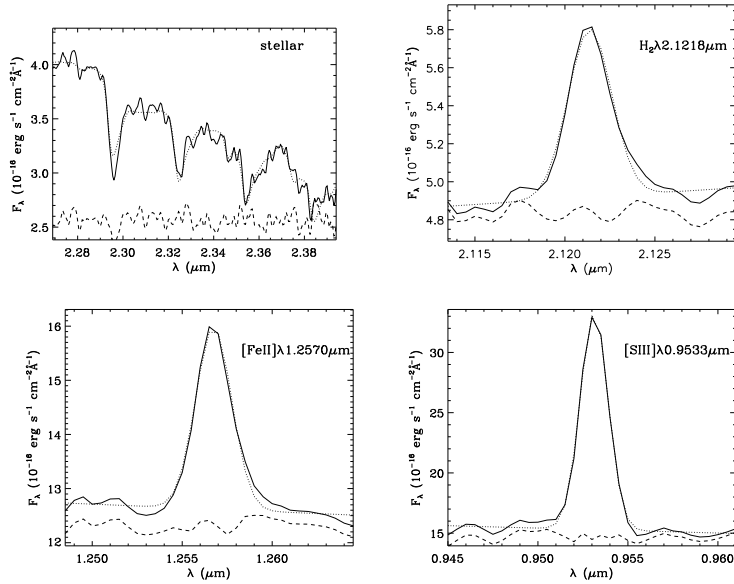


Figure 1. Sample fits of the spectrum of the galaxy NGC 5929. Top left: fit of the stellar absorption spectra to obtain the stellar kinematics. Remaining panels: fit of the emission-line profiles of H₂, [Fe II] and [S III]. The observed spectra are shown as continuous lines, the fits as dotted lines and the residuals as dashed lines.

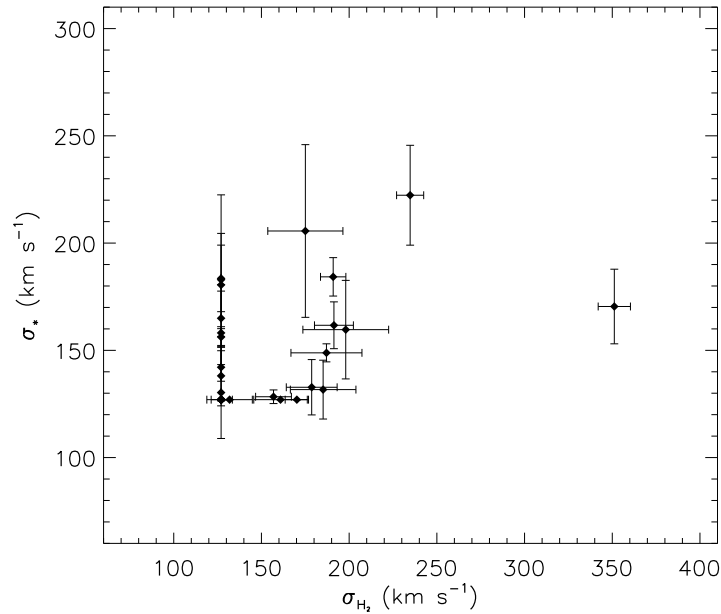


Figure 2. Comparison between the gas velocity dispersions obtained from the H₂ λ2.122 μm emission line (σ_{H_2}) and the stellar velocity dispersions from the CO stellar absorptions at $\sim 2.3 \mu\text{m}$ (σ_*). Points with no error bars in one or both axes represent measurements that are unresolved by our observations and should be considered as upper limits.

were not able to measure one or more values due to the absence of the absorption/emission lines or due to a low signal-to-noise ratio.

We have looked for correlations between the stellar and the gaseous velocity dispersions using the values of Table 1 to construct the graphs of Figures 3, 2 and 4. We have used the IDL routine R_CORRELATE to obtain the Spearman correlation coefficient R for each graph. Figure 2 shows σ_* vs.

Table 1. Stellar and gas velocity dispersions for the galaxies of the sample.

Object	Hubble Type ^a	Nuclear Activity ^a	σ_{\star} (km s ⁻¹)	σ_{H_2} (km s ⁻¹)	$\sigma_{[\text{FeII}]}$ (km s ⁻¹)	$\sigma_{[\text{SIII}]}$ (km s ⁻¹)
MRK334	Sbc	Sy1	<127	<127	180±9	278±14
NGC34	S0/a	Sy2	160±23	198±17	227±19	215±18
NGC262	S0/a	Sy2	–	<127	263±17	245±16
MRK993	Sa	Sy2	132±14	185±10	214±12	287±16
NGC591	SB0/a	Sy2	130±21	<127	274±17	229±14
MRK573	SB0	Sy2	<127	<127	172±12	211±15
NGC1097	SB(s)b	Sy1	165±13	<127	166±12	381±28
NGC1144	E	Sy2	206±40	175±13	230±18	233±18
MRK1066	S0/a	Sy2	<127	<127	206±15	234±17
NGC1275	S0	Sy2	–	173±21	313±38	564±68
NGC1614	SB(s)c	Sb	<127	<127	203±12	217±13
MCG-5-13-17	SB0/a	Sy1	162±11	191±22	162±19	201±23
NGC2110	E-S0	Sy2	184±16	<127	248±17	305±21
ESO428-G014	S0	Sy2	<127	161±11	233±18	253±18
MRK1210	S?	Sy2	181±24	<127	316±32	342±35
MRK124	S?	NLS1	222±23	235±27	335±39	244±29
MRK1239	E-S0	NLS1	–	–	<127	370±35
NGC3227	SB(s)a	Sy1	128±3	157±24	314±48	276±42
H1143-192	–	Sy1	–	–	170±28	410±68
NGC3310	SB(r)bc	Sb	142±18	<127	130±9	153±10
PG1126-041	S	QSO	–	<127	254±34	363±48
NGC4051	SB(rs)bc	NLS1	<127	<127	142±6	215±9
NGC4151	SB(rs)ab	Sy1	136±19	<127	194±41	231±48
MRK766	SB(s)a	NLS1	<127	<127	133±20	188±19
NGC4748	S?	NLS1	<127	170±15	171±21	273±23
TONS0156	–	QSO	–	–	<127	712±200
MRK279	S0	NLS1	138±12	<127	209±49	335±79
NGC5548	S0/a	Sy1	<127	<127	165±43	213±55
MRK478	Sc	NLS1	–	161±22	171±23	390±53
NGC5728	SBa	Sy2	<127	132±23	<127	223±38
PG1448+273	E?	QSO	–	<127	–	303±1
MRK684	Sab	Sy1	170±17	351±18	–	540±27
MRK291	SBa	NLS1	–	129±14	144±16	167±18
MRK493	SBb	NLS1	–	<127	232±12	412±21
NGC5929	Sa	Sy2	158±23	<127	208±26	181±23
NGC5953	S0/a	Sy2	149±4	187±8	289±13	289±13
PG1612+261	–	QSO	166±18	–	266±53	262±52
MRK504	S?	NLS1	<127	<127	–	333±38
3C351	–	BLRG	–	–	–	187±14
ARP102B	E0	Sy1	<127	155±9	195±10	299±16
1H 1934-063	–	NLS1	184±9	191±8	238±11	291±13
MRK509	E-S?	Sy1	<127	–	159±39	370±91
1H2107-097	–	Sy1	<127	–	<127	256±56
ARK564	Sbc	NLS1	–	180±10	176±10	260±15
NGC7469	SBbc	Sy1	–	–	161±15	283±18
NGC7682	SBab	Sy2	183±40	<127	198±27	205±28
NGC7714	SB(s)b	HII	<127	<127	165±13	184±14

^a The Hubble type and Nuclear Activity were taken NASA/IPAC Extragalactic Database (NED) and Hyperleda Database (Paturel et al. 2003).

σ_{H_2} . The range of the σ_{\star} and σ_{H_2} values is approximately the same, something we have noticed in our previous studies of individual galaxies using integral field spectroscopy of the inner hundreds of parsecs (e.g. Riffel et al. 2008, 2009; Riffel & Storchi-Bergmann 2011a,b). Nevertheless, we have obtained only a very weak correlation between σ_{H_2} and σ_{\star} , with $R = 0.35$, but we note that the H₂ line is unresolved for several objects.

The relation between σ_{\star} and $\sigma_{[\text{FeII}]}$ is presented in Figure 3, showing that $\sigma_{[\text{FeII}]}$ is usually higher than σ_{\star} , which is also in agreement with the results from the integral field spectroscopic

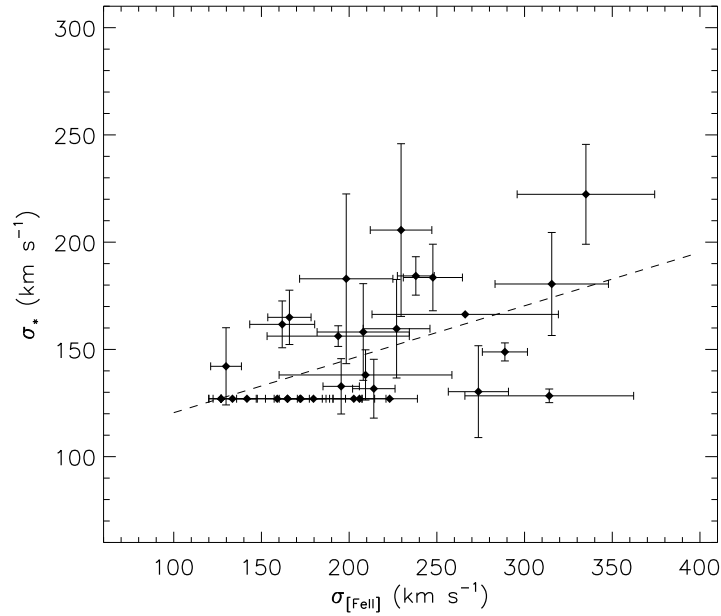


Figure 3. As Fig. 2 but for gas velocity dispersion derived using [Fe II] λ 1.257 μ m. The dashed line represents the best linear fit of the data, given by: $\sigma_{\star} = 95.4 \pm 16.1 + (0.25 \pm 0.08) \times \sigma_{[\text{Fe II}]}$.

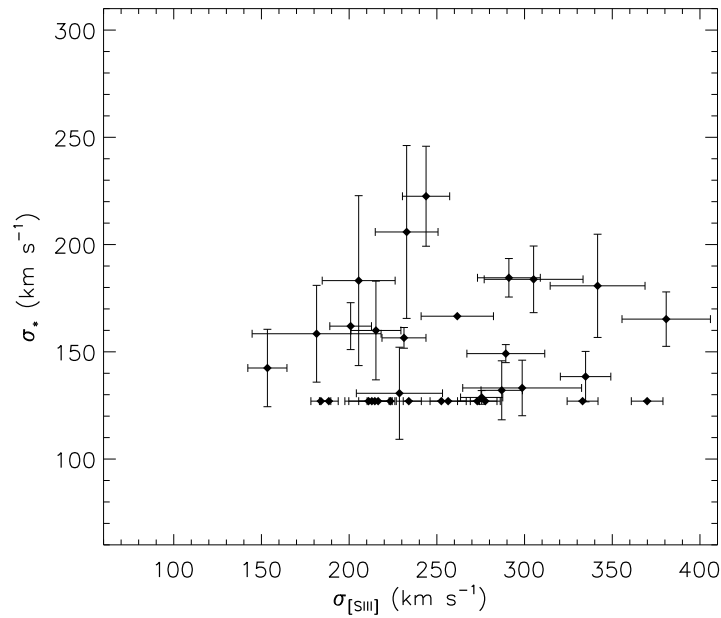


Figure 4. As Fig. 2 but for gas velocity dispersion derived using [S III] λ 0.953 μ m.

studies above. A better correlation is observed between σ_{\star} and $\sigma_{[\text{Fe II}]}$ than with σ_{H_2} , corresponding to a correlation coefficient $R = 0.56$ obtained as described above. We fitted the data by a linear equation of the form $\sigma_{\star} = A + B \times \sigma_{[\text{Fe II}]}$ using the IDL routine `LINMIX_ERR`, which uses a Bayesian approach to linear regression with errors in both variables and takes into account upper limits for the measurements (Kelly 2007). The best fit to the data is given by

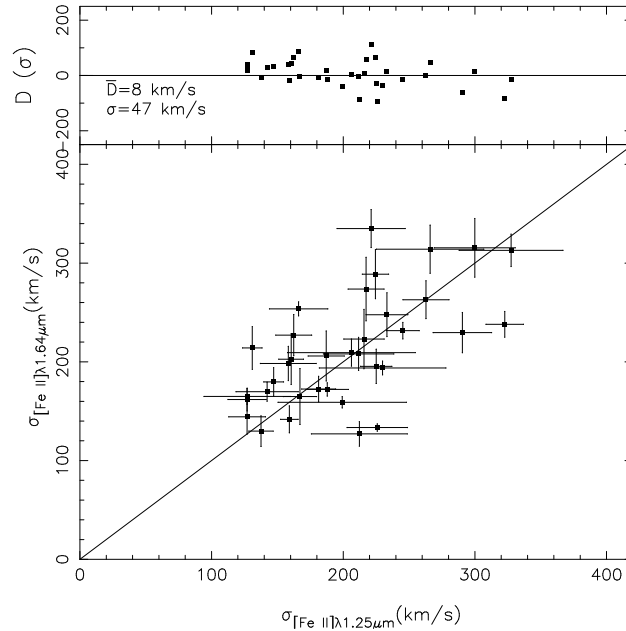


Figure 5. $\sigma_{[\text{Fe II}]\lambda 1.644}$ vs. $\sigma_{[\text{Fe II}]\lambda 1.257}$. The solid line represents a one-to-one relationship. The top panel shows the difference between the values of $\sigma_{[\text{Fe II}]\lambda 1.644}$ and $\sigma_{[\text{Fe II}]\lambda 1.257}$ defined as $D(\sigma) = \sigma_{[\text{Fe II}]\lambda 1.644} - \sigma_{[\text{Fe II}]\lambda 1.257}$, as well as the average value of this difference (\bar{D}).

$$\sigma_{\star} = 95.4 \pm 16.1 + (0.25 \pm 0.08) \times \sigma_{[\text{Fe II}]} \quad (1)$$

which is shown as a dashed line in Fig. 3.

Finally, the relation between σ_{\star} and $\sigma_{[\text{SIII}]}$ is shown in Figure 4, resulting in a correlation coefficient $R = 0.32$, suggesting only a very weak correlation. This figure also shows that $\sigma_{[\text{SIII}]}$ is larger than σ_{\star} by more than a hundred km s^{-1} , on average.

5 DISCUSSION

The use of the velocity dispersion from the Narrow Line Region emission lines as a proxy for σ_{\star} in order to obtain an estimate for the SMBH mass via the $M_{\text{BH}} - \sigma_{\star}$ relation in active galaxies is not new. It has been previously used in the optical domain, where the emission line most commonly used is $[\text{O III}]\lambda 5007$ (e.g. Wu 2009; Salviander et al. 2006; Kaspi et al. 2005; Onken et al. 2004). This emission line has been used instead of σ_{\star} because in active galaxies σ_{\star} cannot be easily measured due to dilution of the stellar absorption lines by the AGN continuum or its scattered light.

In this paper we present an alternative to be used in the near-IR. As shown above, we found a correlation between σ_{\star} and $\sigma_{[\text{Fe II}]}$, indicating that the latter can be used to estimate σ_{\star} using equation 1. $[\text{Fe II}]$ has two similarly strong emission lines which can be observed in the near-IR: $[\text{Fe II}]\lambda 1.257$ in the J band and $[\text{Fe II}]\lambda 1.644$ in the H band. In Figure 5 we present a comparison between the σ of these two lines, where the solid line shows an one-to-one relationship. This

comparison shows that the width of these lines is the same within the errors, with a mean difference of $\sigma_{[\text{Fe II}]\lambda 1.644} - \sigma_{[\text{Fe II}]\lambda 1.257} = 8 \text{ km s}^{-1}$ and a scatter of 47 km s^{-1} , as seen in the top panel of Fig. 5. This scatter may be partially due to the fact that $[\text{Fe II}]\lambda 1.644$ is close in wavelength to Brackett 12, which usually appears in absorption and may affect the measurement of $[\text{Fe II}]$ line.

Why is $\sigma_{[\text{Fe II}]}$ better correlated with σ_{\star} than σ_{H_2} ? As pointed out in the Introduction, our previous studies using Integral field spectroscopy (Riffel et al. 2008, 2009; Riffel & Storchi-Bergmann 2011a,b) showed that the H_2 kinematics frequently shows a rotation pattern and a smaller velocity dispersion than that of the ionized gas. This also led to the conclusion that the H_2 gas was more restricted to the galaxy plane, while the ionized gas – and in particular $[\text{Fe II}]$ – extended to higher galactic latitudes. The integrated value of σ_{\star} from the nuclear region of galaxies is dominated by the contribution of bulge stars, which are not restricted to the plane, showing a “hotter” kinematics. Thus, it can be understood that the velocity dispersion of gas which is restricted to the plane does not correlate with that of bulge stars, while that of gas extending to higher latitudes, similar to those of the bulge – such as the $[\text{Fe II}]$ emitting gas – is correlated to that of the bulge stars. The higher values of $\sigma_{[\text{Fe II}]}$ relative to σ_{\star} are probably due to extra heating provided by a nuclear AGN outflow.

Our results can be compared with previous ones in the optical using the σ of the $[\text{O III}]\lambda 5007$ emission line as a proxy for σ_{\star} . For a sample of 66 Seyfert galaxies, Nelson & Whittle (1996) found a scatter of 0.20 dex around a one-to-one relation between σ_{\star} and $\sigma_{[\text{O III}]}$, while Onken et al. (2004) found a smaller scatter of 0.15 dex for a sample of 16 AGNs, for which 25% of their sources have $\sigma_{[\text{O III}]}$ deviating by more than 0.20 dex from the values expected based on their σ_{\star} . We found a scatter of 0.07 dex between the values obtained via equation 1 and the measured values for σ_{\star} , which is thus smaller than that for $\sigma_{[\text{O III}]}$.

A cautionary note is the observation of recent spatially resolved studies (e.g. our previous studies already mentioned) that the $[\text{Fe II}]$ emission originates at least in part in outflowing gas. Thus, the width of the line is not only due to orbital motion in the gravitational potential of the galaxy, but is also due to broadening by the outflow, what is consistent with the observation that $\sigma_{[\text{Fe II}]}$ is larger than σ_{\star} . Similar outflows – most probably the same – are observed in the $[\text{O III}]$ emitting gas (e.g. Fischer et al. 2011, 2010; Crenshaw et al. 2010, 2009; Crenshaw & Kraemer 2007; Das, Crenshaw & Kraemer 2007; Das et al. 2005). Nevertheless, this line has been frequently used as a proxy for σ_{\star} as discussed above, due to the lack of a better indicator. Our argument is that the $\sigma_{[\text{Fe II}]}$ is at least as good σ_{\star} proxy as $\sigma_{[\text{O III}]}$, and can be used when the latter is not available.

We thus propose the use of $\sigma_{[\text{Fe II}]}$ to obtain σ_{\star} via eq. 1 in cases for which it is not possible to

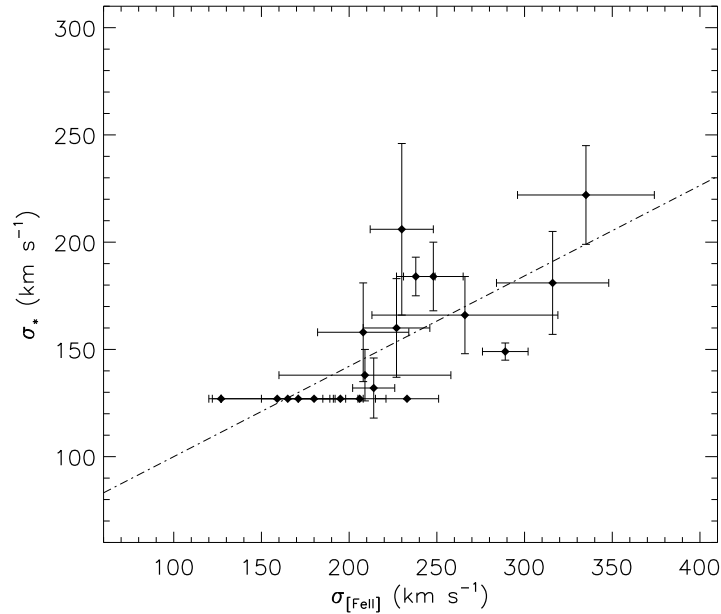


Figure 6. As Fig. 2 but for gas velocity dispersion derived using $[\text{Fe II}]\lambda 1.257\mu\text{m}$ for the sub-sample of unbarred galaxies. The dashed line represents the best linear fit of the data, given by: $\sigma_{\star} = 57.9 \pm 23.5 + (0.42 \pm 0.10) \times \sigma_{[\text{Fe II}]}$.

measure the stellar kinematics of the galaxy, and the optical spectrum is obscured or not available, so that the $[\text{O III}]\lambda 5007$ emission line is also not available. Nevertheless, this suggestion should be used with care, since the $M_{\bullet} - \sigma_{\star}$ is calibrated from a parent sample of mostly early-type galaxies and, as seen in Table 1 most of the objects of our sample are late-type. Late-type galaxies can have distinct σ_{\star} values than early-type galaxies, since the orbits of the stars in a disk are different than the orbits of the stars in the bulge. Additionally, some of the galaxies of our sample have bars, circumnuclear star forming rings or nuclear starbursts or even are classified as peculiar objects and thus the σ_{\star} measured for these objects could be very different than those for the classical bulge, used to calibrate the $M_{\bullet} - \sigma_{\star}$ relationship.

5.1 The effect of galaxy morphology on the $M_{\bullet} - \sigma$ relation

As pointed out above, the $M_{\bullet} - \sigma_{\star}$ relation is calibrated using a parent sample of mostly early-type galaxies. But Table 1 shows that about 30% of the galaxies of our sample are late-type, which can have distinct σ_{\star} values from those of early-type galaxies, since the orbits of the stars in a disk (which dominate in late-type galaxies) are distinct from those in a bulge (which dominate in early-type galaxies). Additionally, $\approx 30\%$ of the galaxies of our sample have bars, and another 30% have uncertain classifications and are peculiar objects which may not obey the the $M_{\bullet} - \sigma_{\star}$ relationship.

Xiao (2011) investigated the $M_{\bullet} - \sigma_{\star}$ relation for late-type galaxies for a sample of 93 objects with Seyfert 1 nucleus. They examined the $M_{\bullet} - \sigma_{\star}$ relationship for subsamples of barred and unbarred host galaxies and found no difference in slope. They only found a mild offset in the relation between low- and high-inclination disk galaxies, with the latter tending to have larger σ_{\star} for a given value of the black hole mass.

The $M_{\bullet} - \sigma_{\star}$ relationship for galaxies of different Hubble types have also been studied by Graham et al. (2011) using a sample of 64 galaxies. They found that restricting the sample only to elliptical galaxies, or only to non-barred galaxies result in tighter relations (with less scatter) and a smaller slope than when using the full sample of galaxies. The $M_{\bullet} - \sigma_{\star}$ relation obtained when the sample is restricted to barred galaxies only lies ≈ 0.45 dex below the relation obtained for elliptical and non-barred galaxies.

In order to investigate the effect of the presence of a bar in the $M_{\bullet} - \sigma_{[\text{Fe II}]}$ relation of Fig. 3, we divided our sample into two sub-samples: one composed of barred galaxies only and the other of unbarred galaxies. We found a much better correlation between $\sigma_{[\text{Fe II}]}$ and σ_{\star} for the unbarred galaxies than for the total sample, as illustrated in Fig.6. The correlation coefficient is $R = 0.80$ and a linear regression to the relation is given by

$$\sigma_{\star} = 57.9 \pm 23.5 + (0.42 \pm 0.10) \times \sigma_{[\text{Fe II}]} \quad (2)$$

On the other hand, no correlation was found for the barred galaxies, for which the correlation coefficient between $\sigma_{[\text{Fe II}]}$ and σ_{\star} is only $R = 0.20$.

Approximately half of our sample is composed by early-type galaxies (half of which are barred), the remainder being of late-type galaxies and galaxies with uncertain morphology (usually because they are distant and compact). But the number of galaxies of our sample is not large enough to further investigate the effect of morphology (besides the effect of bars discussed above) on the $\sigma_{\star} - \sigma_{[\text{Fe II}]}$ relation. This will be possible only when more near-IR AGN spectra become available, and the equations 1 and 2 could be better calibrated using large non-biased samples of galaxies.

On the other hand, when applying the $\sigma_{\star} - \sigma_{[\text{Fe II}]}$ relation to distant galaxies, it will be hard to ascertain a Hubble type to such galaxies, and it will probably better to just use the relation for the whole sample (equation 1), in spite of the fact that a relation for restricted Hubble types (e.g., for galaxies without bars) shows less scatter.

Many present/future missions are discovering/will discover large numbers of obscured AGN, such as the Wise mission

(http://www.nasa.gov/mission_pages/WISE/news/wise20120829.html) or the Vista Variables in the Via Lactea survey

(http://mwm.astro.puc.cl/mw/index.php/Main_Page), which are potential samples to benefit from the relation we have found in order to obtain the SMBH masses, if [Fe II] emission lines are present in the spectra.

5.2 Estimating SMBH masses using $\sigma_{[\text{Fe II}]}$

We now evaluate the effect of the scatter introduced by the use of eq. 1 in the value of SMBH masses obtained via the $M_{\bullet} - \sigma_{\star}$ relation, which result in higher uncertainties in M_{\bullet} than those obtained by using σ_{\star} directly. In order to do this, we use the relation below from Graham et al. (2011):

$$\log(M_{\bullet}/M_{\odot}) = (8.13 \pm 0.05) + (5.13 \pm 0.34)\log[\sigma_{\star}/200 \text{ km s}^{-1}]. \quad (3)$$

to obtain M_{\bullet}/M_{\odot} , using for σ_{\star} first its measurement from the stellar kinematics and then the value derived from $\sigma_{[\text{Fe II}]}$ using eq. 1. We compare the two values in Figure 7 ($\log M(\sigma_{\star})$ vs. $\log M(\sigma_{[\text{Fe II}]})$), which shows a good agreement between them, with an average difference of $\Delta \log M_{\bullet} = \log M(\sigma_{[\text{Fe II}]}) - \log M(\sigma_{\star}) = 0.02 \pm 0.32$. In the same figure, we show also the masses for the SMBH obtained for the sub-sample of unbarred galaxies as open symbols, using the eq. 2 to obtain σ_{\star} . There is no difference in the average value of the SMBH masses obtained, and the mean scatter is 0.28 dex, which is somewhat smaller than the one for the complete sample.

6 CONCLUSIONS

We have used near-infrared spectroscopic data of a sample of 47 active galaxies in order to investigate possible correlations between the stellar velocity dispersion (σ_{\star}), obtained from the fit of the K-band CO absorption band-heads, and the gas velocity dispersion (σ) obtained from the fit of the profiles of the [S III] $\lambda 0.95332\mu\text{m}$, [Fe II] $\lambda 1.25702\mu\text{m}$, [Fe II] $\lambda 1.644\mu\text{m}$ and H₂ $\lambda 2.12182\mu\text{m}$ emission lines. The main conclusions of the present paper are:

- Very weak correlations are found between σ_{\star} and both σ_{H_2} and $\sigma_{[\text{S III}]}$;
- The best correlation is found for the [Fe II] emitting gas with $R = 0.58$ for the Spearman rank correlation coefficient between σ_{\star} and $\sigma_{[\text{Fe II}]}$ (both the $\lambda 1.257\mu\text{m}$ and $\lambda 1.644\mu\text{m}$ emission lines can be used). A better correlation is found if we exclude the barred galaxies from the sample ($R=0.80$), while no correlation is found for the sub-sample of barred galaxies.

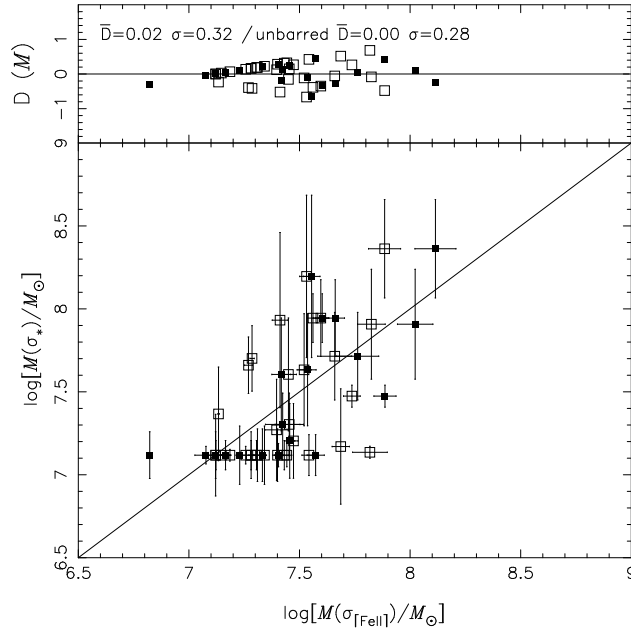


Figure 7. Comparison between SMBH mass values obtained directly from the relation with σ_* (y-axis) and using $\sigma_{[\text{Fe II}]}$ (x-axis) to obtain σ_* . The filled squares are for the complete sample, for which the eq. 1 was used and the opened squares points of for unbarred galaxies, for which the eq. 2 was used. The error bars shown include the uncertainties in the calibration of the $M_\bullet - \sigma_*$ relation.

- $\sigma_{[\text{Fe II}]}$ can thus be used to estimate σ_* for objects for which the stellar velocity dispersion cannot be measured or is unknown. The best fit of the data is given by the equation $\sigma_* = 95.4 \pm 16.1 + (0.25 \pm 0.08) \times \sigma_{[\text{Fe II}]}$ for the complete sample and $\sigma_* = 57.9 \pm 23.5 + (0.42 \pm 0.10) \times \sigma_{[\text{Fe II}]}$ for the sub-sample of unbarred galaxies.
- The equations above should be improved and re-calibrated when larger and non-biased samples of near-IR spectra of AGN become available.
- The scatter from a one-to-one relationship between σ_* and its value derived from $\sigma_{[\text{Fe II}]}$ using the equation above for our sample is 0.07 dex, which is smaller than the scatter of previous relations using $\sigma_{[\text{O III}]}$ in the optical as a proxy for σ_* .
- The use of $\sigma_{[\text{Fe II}]}$ in the near-IR instead of $\sigma_{[\text{O III}]}$ in the optical is particularly important for cases in which the optical spectra is not available or is obscured, as is the case of many AGN.
- The comparison of the masses for SMBHs obtained from the direct use of σ_* in the $M_\bullet - \sigma_*$ relation with those using $\sigma_{[\text{Fe II}]}$ to obtain σ_* reveals only a small average difference of $\Delta \log M_\bullet = 0.02 \pm 0.32$ for the complete sample and $\Delta \log M_\bullet = 0.00 \pm 0.28$ excluding barred galaxies from the sample.

ACKNOWLEDGEMENTS

We thank an anonymous referee for useful suggestions which helped to improve the paper. This paper is based on observations obtained at the Infrared Telescope Facility, which is operated by the University of Hawaii under Cooperative Agreement no. NNX-08AE38A with the National Aeronautics and Space Administration, Science Mission Directorate, Planetary Astronomy Program. This research has made use of the NASA/IPAC Extragalactic Database (NED) which is operated by the Jet Propulsion Laboratory, California Institute of Technology, under contract with the National Aeronautics and Space Administration. We acknowledge the usage of the HyperLeda database (<http://leda.univ-lyon1.fr>). This work has been partially supported by the Brazilian institution CNPq and FAPERGS.

REFERENCES

- Booth, C. M.; Schaye, J., 2011, *MNRAS*, 413, 1158
- Bower, R. G. et al. 2006, *MNRAS*, 370, 645.
- Cappellari, M. & Emsellem, E., 2004, *PASP*, 116, 138.
- Crenshaw, D. M., Kraemer, S. B., 2007, *ApJ*, 659, 250.
- Crenshaw, D. M., Kraemer, S. B., Schmitt, H. R., Kaastra, J. S., Arav, N., Gabel, J. R., Korista, K. T., 2009, *ApJ*, 698, 281.
- Crenshaw, D. M., Kraemer, S. B., Schmitt, H. R., Jaffé, Y. L., Deo, R. P., Collins, N. R., Fischer, T. C., 2010, *AJ*, 139, 871.
- Das, V., Crenshaw, D. M., Kraemer, S. B., 2007, *ApJ*, 656, 699.
- Das, V., Crenshaw, D. M., Hutchings, J. B., Deo, R. P., Kraemer, S. B., Gull, T. R., Kaiser, M. E., Nelson, C. H., Weistrop, D., 2005, *AJ*, 130, 945.
- Das, V., Crenshaw, D. M., Kraemer, S. B., 2007, *ApJ*, 656, 699.
- Di Matteo, T., Springel, V. & Hernquist, L. 2005, *Nature*, 433, 604.
- Ferrarese, L. & Ford, H. C., 2005, *Space Science Reviews*, 116, 523.
- Ferrarese, L. & Merrit, D., 2000, *ApJ*, 547, 140.
- Fischer, T. C., Crenshaw, D. M., Kraemer, S. B., Schmitt, H. R., Mushotsky, R. F., Dunn, J. P., 2011, *ApJ*, 727, 71.
- Fischer, T. C., Crenshaw, D. M., Kraemer, S. B., Schmitt, H. R., Trippe, M. L., 2010, *AJ*, 140, 577.
- Gebhardt, K. et al. 2000, *ApJ*, 539, 13.

- Graham, A. W., Onken, C. A., Athanassoula, E., Combes, F., 2011, MNRAS, 412, 2211.
- Greene, J. E., & Ho, L. C., 2005, ApJ, 630, 122.
- Greene, J. E., & Ho, L. C., 2006, ApJ, 641, L21.
- Jahnke, K. & Maccio, A. V. 2011, ApJ, 734, 92.
- Kaspi, S., Maoz, D., Netzer, H., Peterson, B. M., Vestergaard, M., & Jannuzi, B. T., 2005, ApJ, 629, 61.
- Kelly, B. C., 2007, ApJ, 665, 1489.
- Magorrian, J. et al. 1998, AJ, 115, 2285.
- Nelson, C. H., & Whittle, M., 1996, ApJ, 465, 96.
- Nemmen R., Bower, R., Babul, A. & Storchi-Bergmann, T. 2007, MNRAS, 377, 1652
- Onken, C. A., Ferrarese, L., Merritt, D., Peterson, B. M., Pogge, R. W., Vestergaard, M., & Wandel, A., 2004, ApJ, 615, 645.
- Paturel, G., Petit, C., Prugniel, Ph., Theureau, G., Rousseau, J., Brouty, M., Dubois, P., Cambrésy, L., 2003, A&A, 412, 45.
- Peterson, B. M., 2008, NewAR, 52, 240.
- Richstone, D. et al., 1998, Nature, 395, A14.
- Riffel, Rogemar A & Storchi-Bergmann, T., 2011a, MNRAS, 411, 469.
- Riffel, Rogemar A & Storchi-Bergmann, T., 2011b, MNRAS, 417, 2752.
- Riffel, Rogemar A., 2010, Ap&SS, 327, 239.
- Riffel, Rogemar A., Storchi-Bergmann, T. & Nagar, N. M., 2010, MNRAS, 404, 166.
- Riffel, Rogemar A., Storchi-Bergmann, T., Dors, O. L., Winge, C., 2009, MNRAS, 393, 378.
- Riffel, Rogemar A., Storchi-Bergmann, T., Winge, C., McGregor, P. J., Beck, T., Schmitt, H., 2008, MNRAS, 385, 1129.
- Riffel, Rogemar A., 2010, Ap&SS, 327, 239.
- Riffel, Rogemar A., Sorchi-Bergmann, T., Winge, C., Barbosa, F. K. B., 2006, MNRAS, 373, 2.
- Riffel, R., Rodríguez-Ardila, A. & Pastoriza, M. G., 2006, A&A, 457, 61.
- Rodríguez-Ardila, A., Contini, M., & Viegas, S. M., 2005, MNRAS, 357, 220.
- Rodríguez-Ardila, A., Pastoriza, M. G., Viegas, S. M., Sigut, T. A. A., & Pradham, A. K., 2004, A&A, 425, 457.
- Salviander, S., Shields, G. A., Gebhardt, K., Bonning, E. W., 2006, NewAR, 50, 803.
- Springel, V., Di Matteo, T. & Hernquist, L., 2005, ApJ, 620, 79.
- Storchi-Bergmann, T., Winge, C., Ward, M. & Wilson, A. S., 1999, MNRAS, 304, 35.
- Storchi-Bergmann, T., McGregor, P. Riffel, Rogemar A., Simões Lopes, R., Beck, T., Dopita, M.,

2009, MNRAS, 394, 1148.

Storchi-Bergmann, T., Simões Lopes, R., McGregor, P. Riffel, Rogemar A., Beck, T., Martini, P.,
2010, MNRAS, 402, 819.

Storchi-Bergmann, T., 2010, Proceedings of the IAU meeting 267: Co-Evolution of Central Black
Holes and Galaxies, 267, 290.

Tremaine, S. et al. 2002, ApJ, 574, 740.

Vestergaard, M., & Peterson, B. M., 2006, ApJ, 641, 689.

Xiao, T., Barth, A. J., Greene, J. E., Ho, L. C., Bentz, M., C., Ludwig, R. R., & Jiang, Y., 2011,
ApJ, 739, 28.

Winge, C., Riffel, Rogemar A., & Storchi-Bergmann, T., 2009, ApJS, 185, 186.

Wu, Q., 2009, MNRAS, 398, 1905.